ACADEMIA ROMÂNĂ
Revue Roumaine de Chimie
https://www.icf.ro/rrch/

Rev. Roum. Chim.,
2023, *68*(10–12), 569–576
DOI: 10.33224/rrch.2023.68.10-12.09

THE POWER OF NOVEL MORPHOLINYL MANNICH BASES TO PROTECT N80 STEEL AGAINST CORROSION IN ACIDIC ENVIRONMENT: DFT AND SAR INVESTIGATIONS

Khaoula KOUCHKAR,[a] Adel KHIOUANI,[b,*], Salah Eddine HACHANI,[c] Youcef BOUMEDJANE,[a] Abdelhek MEKLID[d] and Sofiane MAKHLOUFI[a,e]

[a]Laboratory of Molecular Chemistry and Environment, University of Biskra, BP 145, 07000, Biskra, Algeria
[b]Laboratory of Chemistry of Materials and Living Organisms Activity and Reactivity (LCMVAR), Faculty of Material Sciences, Department of Chemistry, University of Batna 1, Algeria
[c]Department of Process Engineering & Petrochemistry, Faculty of Technology, University of El Oued, El Oued, 39000, Algeria
[d] Laboratory of Applied Chemistry, University of Biskra, BP 145, 07000 Biskra, Algeria
[e]Faculty of Science and Technology, Ziane Achour University of Djelfa, BP 3117, Algeria

Received April 7, 2023

In this research article, we investigate the corrosion inhibition properties of two novel morpholinyl mannich bases namely 3-morpholino-1-phenylpropan-1-one (MB1) and 3-morpholino-1-phenyl-3-(pyridin-4-yl) propan-1-one (MB2). To establish a link between their corrosion inhibition efficacy and molecular characteristics, we employ a comprehensive approach involving the calculation of DFT-derived global and local reactivity parameters, as well as structure-activity relationship (SAR) indices. The obtained values of the global reactivity indices including dipole moment, energy gap, hardness, and softness show a positive correlation with the experimental data earlier reported. Fukui functions give a comprehensive reactive scheme exhibiting the atoms responsible for the electronic transfer. SAR parameters such as molecular volume (V), surface area (SA), and the polarizability (α) were found to be in good accordance with the experimental inhibition effectiveness order.

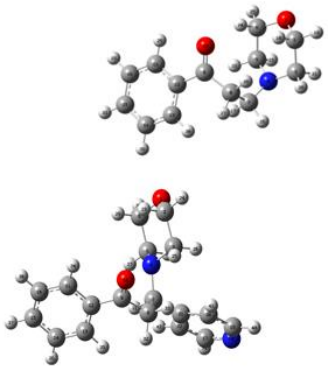

INTRODUCTION

N80 steel is a high-strength and high-toughness carbon seamless steel pipe. This engineering material is extensively used to transport oil and gas from the source rock to the wellhead.[1] During utilization and cleaning process, N80 steel can be corroded by exposure its surface to atmosphere or in contact with different aggressive media such as aqueous and acidic solutions which leads to reduce dramatically its properties and its performance.[2]

The prevention of N80 steel against corrosion became a great task for both academia and industry. The use of corrosion inhibitors is the most effective solution to avoid corrosion. Natural or synthesized organic molecules containing heteroatoms having free electron pairs, aromatic rings, or conjugated systems are predicted to be the

* Corresponding author: adel.khiouani@univ-batna.dz

best inhibitor candidates thanks to their high ability to adhere on the metallic surface leading to prohibiting the corrosion phenomena.[3]

Experimental techniques such as scanning electron microscopy, electrochemical noise, and electrochemical impedance spectroscopy as well as weight loss measurements are very beneficial to quantify the corrosion inhibition efficacies and comprehending the inhibition mechanisms. However, these above-mentioned laboratory methods are expensive and time requiring.[4]

In recent times, computational chemistry is proved to be the best alternative tool used to understand and predict the relative corrosion inhibition effectiveness of the tested molecules. Theoretical approaches such as density functional theory DFT are very popular for the estimation of chemical reactivity by calculating quantum descriptors namely global reactivity indices such as chemical potential, electronegativity, hardness, softness, and the number of electron transferred from the inhibitor to the metal, these descriptors are directly related to the energy values of HOMO and LUMO frontier molecular orbitals.[5]

Fukui function analysis is a powerful theoretical approach used in the field of corrosion inhibitors to gain deeper insights into the molecular mechanisms underlying inhibition activity. Corrosion inhibitors are compounds designed to mitigate the degradation of metals caused by chemical reactions with their environment, primarily in aggressive environments like aqueous solutions. Fukui function analysis, often based on Density Functional Theory (DFT), helps elucidate the reactivity of specific atoms within a molecule and their influence on inhibiting corrosion processes.[6,7]

Structure-Activity Relationship (SAR) analysis is a valuable tool in the field of corrosion inhibitors, aimed at establishing a mathematical relationship between the molecular structure of inhibitor compounds and their observed inhibitory activity against metal corrosion. SAR analysis helps to predict the inhibition efficiency of new compounds based on their structural features, thus aiding in the rational design and optimization of corrosion inhibitors.[8,9]

In a recent paper, Y. Chen *et al*. have synthesized two novel morpholinyl mannich bases namely 3-morpholino-1-phenylpropan-1-one (MB1) and 3-morpholino-1-phenyl-3-(pyridin-4-yl) propan-1-one (MB2) and then investigated their inhibitory performance against N80 steel corrosion in 1.0 M HCl solution using several laboratory techniques.[10] However, there is no computational work has been performed yet to comprehend the experimental observation related to the previous study. The research paper in hand aims to bridge the gap between the experimental inhibition activities early reported of the concerned inhibitor molecules and their electronic properties using DFT and SAR investigations.

COMPUTATIONAL DETAIL

Global reactivity descriptors

Quantum chemical calculations were carried out using Gaussian 09.[11] After building the molecular structure of the studied inhibitors by Gauss View software, the full optimization started from determining the most stable conformer using the molecular mechanics force fields (MM+) then the obtained results from this theoretical level were further re-optimized using the density functional theory (DFT) with B3LYP hybrid functional method combined with STO-3G, 6-31G, 6-31G++, 6-31G++(d,p) and 6-311G++(d,p) basis sets, respectively, to guarantee obtaining reliable theoretical outcomes able to add an effective correlation at a reasonable computational time. To achieve the calculations in water as a solvent, a self-consistent reaction field (SCRF) with a polarized continuum model (PCM) has been implanted as a keyword in the selected software.[11]

The obtained theoretical outcomes were used to calculate the global reactivity descriptors. According to Koopmans' theory, the ionization potential (I) and the electronic affinity (A) are directly obtained from HOMO and LUMO energy values as described in the following mathematical relations:[12]

$$I = -E_{HOMO} \tag{1}$$

$$A = -E_{LUMO} \tag{2}$$

Pearson's equations permit to quantify quantum parameters including the electronegativity (χ), the the chemical hardness (η) and its inverse; the softness (σ) are given as:[13]

$$\chi = \frac{I + A}{2} \tag{3}$$

$$\eta = \frac{I - A}{2} \tag{4}$$

$$\sigma = \frac{1}{\eta} \quad (5)$$

The fraction of electrons transferred (ΔN) from the inhibitor to mild steel was calculated using Pearson's formula drafted with global hardness and the electronegativity equalization principle:[13]

$$\Delta N = \frac{\chi_{Fe} - \chi_{in}}{2(\eta_{Fe} + \eta_{in})} \quad (6)$$

In the above formula (6), χ_{Fe} and χ_{in} are dedicated both electronegativities of bulk iron and the inhibitor, respectively. η_{Fe} and η_{in} represents the absolute hardness of bulk iron and the inhibitor candidate, respectively, where χ_{Fe} = 7 eV and η_{Fe} = 0 eV.[14]

Local reactivity indices

The local reactivity has been estimated by analyzing Fukui functions to localize the active atoms for the electron transfer in the molecules under investigation. Fukui functions were calculated at DFT level of theory combined with Becke exchange plus Lee-Yang-Parr correlation (B3LYP) functional and 6-311G++ (d,p) basis set. Fukui indices for a site A in the concerned inhibitors can be calculated using the atomic population (p) or the atomic charge (q) like Mulliken charge or CHELPG charge as follows:

For nucleophilic attack: .

$$F^{+} = q^{A}_{N+1} - q^{A}_{N} \quad (8)$$

For electrophilic attack:

$$F^{-} = q^{A}_{N} - q^{A}_{N-1} \quad (9)$$

N, *N*–1, and *N*+1 are referred to the neutral, cationic, and anionic forms of the studied molecules.[15]

SAR calculations

Structure activity relationship SAR indices including surface area (SA), molecular volume (*V*), polarizability (α), and partition coefficient (log *P*) were calculated using HyperChem 8.0 software.

RESULTS AND DISCUSSION

Global reactivity outcomes

The inhibition effects of two novel morpholinyl mannich bases namely 3-morpholino-1-phenylpropan-1-one (MB1) and 3-morpholino-1-phenyl-3-(pyridin-4-yl) propan-1-one (MB2) on N80 steel corrosion in 1.0 M HCl solution have been investigated using gravimetric and electrochemical methods.[10] The data related the experimental tests are collected in Tables 1 and 2.

Table 1

Corrosion parameters obtained by weight loss measurements of N80 steel in 1.0 M HCl containing 350 ppm of MB1 and MB2 inhibitors at 305 K[10]

	C_R (mg·cm^{-2}·h^{-1})	θ	IE (%)
Blank	1.86	-	-
MB1	0.17	0.907	90.7
MB2	0.14	0.925	92.5

Table 2

Electrochemical parameters obtained from polarization curves for N80 steel containing 300 ppm of MB1 and MB2[10]

	I_{corr} (μA cm^{-2})	$-E_{corr}$ (mV)	βa (mV)	−βc (mV)	θ	IE (%)
Blank	777.90	420	101	139	-	-
MB1	75.78	405	69	122	0.9026	90.26
MB2	74.19	401	68	119	0.9046	90.46

The reported experimental outcomes revealed that the inhibition efficiency of these tested molecules follows the order: MB2 > MB1.[10]

In this present investigation, DFT calculations in the gas phase and the aqueous phase have been performed to provide more insights at the molecular level to well understand the experimental inhibition role of the studied morpholinyl mannich bases. Tables 3 and 4 collect the global reactivity indices of these molecules. The optimized molecular structures of the inhibitors under probe as well as the electronic distribution of HOMO and LUMO in these molecules at B3LYP/6-311G++ (d,p) calculation level are shown in Fig. 1.

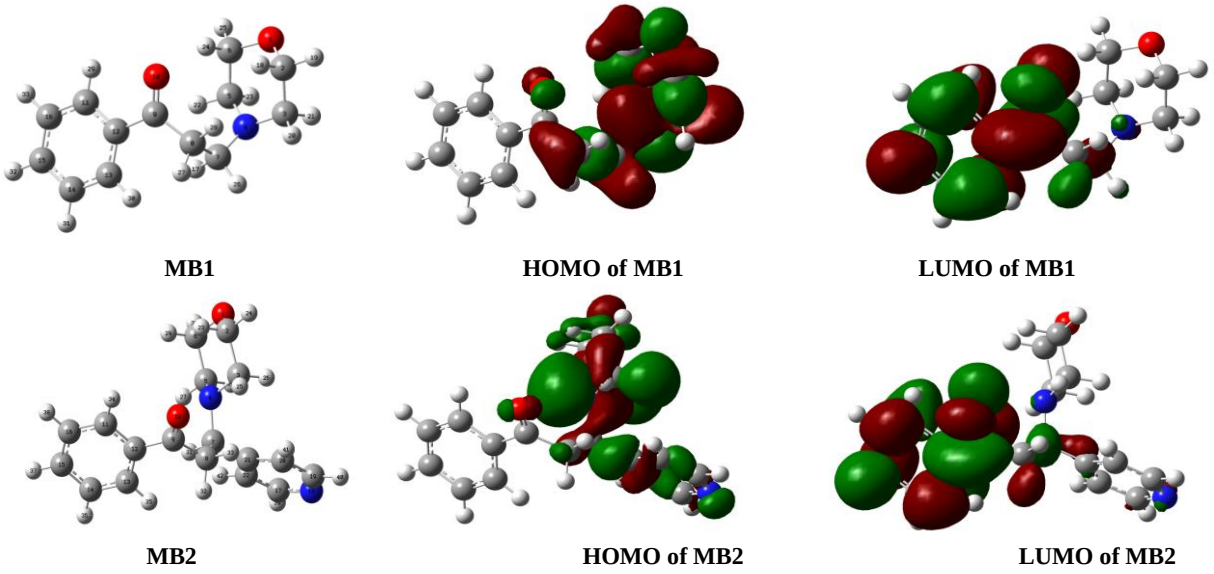

Fig. 1 – Optimized molecular structures of MB1 and MB2 inhibitors and their electronic distributions of HOMO and LUMO orbitals calculated at DFT/B3LYP/6-311G++(d,p) in aqueous phase.

Table 3

Global chemical reactivity descriptors of the inhibitor molecules calculated in gas phase

	μ	E_H	E_L	ΔE	I	A	χ	η	σ	ΔN
STO-3G										
MB1	2.814	-2.752	0.782	-3.534	2.752	-0.782	0.985	1.767	0.566	1.703
MB2	2.577	-3.615	0.935	-4.551	3.615	-0.935	1.340	4.083	0.245	0.693
6-31G										
MB1	4.223	-5.667	-1.648	-4.019	5.667	1.648	3.658	2.010	0.498	0.832
MB2	4.798	-5.783	-1.826	-3.957	5.783	1.826	3.805	1.978	0.506	0.808
6-31G++										
MB1	4.393	-5.990	-1.998	-3.992	5.990	1.998	3.994	1.996	0.501	0.753
MB2	4.625	-6.092	-2.169	-3.922	6.092	2.169	4.131	1.961	0.510	0.732
6-31G++(d,p)										
MB1	3.794	-5.217	-1.891	-3.326	5.217	1.891	3.554	1.663	0.601	1.036
MB2	3.987	-6.240	-2.012	-4.228	6.240	2.012	4.126	2.114	0.473	0.680
6-311G++(d,p)										
MB1	3.748	-6.230	-1.876	-4.354	6.230	1.876	4.053	2.177	0.459	0.677
MB2	3.915	-6.279	-2.025	-4.254	6.279	2.025	4.152	2.127	0.470	0.670

Table 4

Global chemical reactivity descriptors of the inhibitor molecules calculated in solvent phase

	μ	E_H	E_L	ΔE	I	A	χ	η	σ	ΔN
STO-3G										
MB1	2.813	-2.916	0.788	-3.704	2.916	-0.788	1.064	1.852	0.540	1.603
MB2	2.968	-3.673	0.920	-4.593	3.673	-0.920	1.376	2.297	0.435	1.224
6-31G										
MB1	5.772	-5.795	-1.767	-4.028	5.795	1.767	3.781	2.014	0.497	0.799
MB2	5.963	-5.835	-1.829	-4.006	5.835	1.829	3.832	2.003	0.499	0.791
6-31G++										
MB1	6.307	-6.083	-2.113	-3.969	6.083	2.113	4.098	1.985	0.504	0.731
MB2	6.258	-6.122	-2.160	-3.962	6.122	2.160	4.141	1.981	0.505	0.722
6-31G++(d,p)										
MB1	5.986	-5.476	-2.001	-3.475	5.476	2.001	3.738	1.738	0.576	0.939
MB2	5.442	-6.260	-2.004	-4.256	6.260	2.004	4.132	2.128	0.470	0.674
6-311G++(d,p)										
MB1	5.919	-5.518	-2.023	-3.495	5.518	2.023	3.771	1.748	0.572	0.924
MB2	5.332	-6.297	-2.021	-4.276	6.297	2.021	4.159	2.138	0.468	0.665

The dipole moment (μ) could inform about the polarity of the tested chemical species. A molecule having dipole moment value different than zero is a polar molecule and vice versa.[16] The dipole moment is a beneficial reactivity parameter; the higher the dipole moment is the greater is the tendency of a molecule to adhere into the metal to protect its surface against aggressive agents.[16] Besides, the studies have reported that an increase in the inhibition efficiency of the inhibitors with the increase of dipole moment increases with. The dipole moment (μ) values collected in Table 3 increased as follows: MB1 < MB2. This result is in full agreement with the experimental findings.

According to frontier molecular orbital concept (FMO) proposed by Fukui Kinachi,[17] the electron transfer is ascribed to the interactions between the highest occupied molecular orbital (HOMO) and lowest unoccupied molecular orbital (LUMO) of the tested reagents. The power of an inhibitor candidate to bind a metal surface increases with the increment of its HOMO energy value (E_H). Therefore, higher inhibition effectiveness is expected.[17] The (E_H) data displayed in Tables 3 and 4 revealed that the inhibitor MB2 has lower HOMO energy compared to that of MB1 which is in contradiction with the experimental results of the inhibition efficacy earlier reported.

The chemical reactivity of the inhibiting molecules can be also estimated using another important quantum descriptor namely the energy gap (ΔE); the difference between HOMO and LUMO energy values. A molecule has the least energy gap is predicted to have the highest chemical reactivity[18] and therefore protects the metal surface better than other inhibitor compounds. Our theoretical outcomes given in Table 4 show that the energy gap values of the studied inhibitors decreased in the order MB1 > MB2, which is in full agreement with the experimental findings.

The chemical hardness (η) and its reciprocal the chemical softness (σ) are two reactivity indicators; the hardness quantifies the resistance of a molecule to the deformation or the polarization of the electron cloud induced by a chemical reaction.[19] The inhibiting molecules having lower chemical hardness values are powerful in terms of metal protection therefore higher inhibition efficiency is expected. The results shown in Table 3 declared that the chemical hardness related to the tested molecules follow the trend: MB1 > MB2 and the softness follow the inverse trend: MB2 > MB1. These results emphasize the order of the experimental inhibition efficiency previously reported.

The electronegativity (χ) represents the tendency of an atom in a molecule to attract the shared pair of electron to itself. This quantum index is beneficial to evaluate the reactivity of the inhibitor under probe.[16] The studies demonstrated that the molecules with lower electronegativity values are considered as excellent corrosion inhibitors therefor higher inhibition activity is expected.[20] The data of Tables 3 and 4 confirmed that the electronegativity (χ) follows the sequence: MB1 < MB2 indicating that our result does not validate the experimental observations.

On its part, the number of electrons transferred (ΔN) from the inhibitor candidate to the metal surface was calculated and listed in Tables 3 and 4. According to Lukovits and al, the inhibiting molecule could give electrons to the deficient metal surface if is positive and less than 3.6.[21] Higher value of ΔN indicates higher tendency of the inhibitor to offer electrons to the poor d orbital of the metallic surface leading to maximum protection against corrosion. As can be seen in Tables 3 and 4, the values of (ΔN) indicate that the investigated molecules are electron donor to the poor metal surface, the electron donation obeys the order MB1 > MB2 which is in negative correlation with the experimental outcomes.

Local reactivity outcomes

The electronic transition process occurs via electron donor-acceptor interactions between the metal centers and the inhibitors. Fukui function analysis could give a reactive scheme allowing localizing the atoms contributing in the electron transfer between the inhibitor candidate and the metal surface. The privileged site for the nucleophilic attack is reserved to the atom with higher f^+ values while the atom possessing higher f^- is considered as the preferred site for the electrophilic attack.[22] The calculated Fukui functions corresponding to the studied inhibitors are given in Table 5.

Table 5

Fukui functions of the studied inhibitors considering Mulliken charges calculated in solvent phase

MB1					MB2				
Atoms	P^+	P^-	f^+	f^-	Atoms	P^+	P^-	f^+	f^-
O1	-0,203	-0,101	0,092	0,011	O1	-0,180	-0,099	0,076	0,081
C2	-0,308	-0,330	-0,007	-0,015	C2	-0,570	-0,613	-0,037	-0,043
C3	-0,212	-0,306	-0,086	-0,008	C3	-0,045	-0,112	-0,067	-0,067
N4	0,056	0,358	0,305	-0,003	N4	0,484	0,701	0,243	0,217
C5	-0,030	-0,191	-0,105	-0,056	C5	-0,039	-0,155	-0,080	-0,116
C6	-0,495	-0,452	0,003	0,040	C6	-0,461	-0,527	-0,066	-0,065
C7	-0,626	-0,702	-0,080	0,004	C7	-0,619	-0,598	-0,036	0,022
C8	0,237	0,071	-0,087	-0,079	C8	0,092	-0,036	-0,057	-0,128
C9	-0,831	-0,755	0,054	0,022	C9	-1,445	-1,432	0,015	0,009
O10	-0,484	-0,242	0,040	0,202	O10	-0,468	-0,211	0,043	0,257
C11	0,266	0,386	-0,009	0,128	C11	0,046	0,163	0,014	0,117
C12	1,238	1,281	-0,016	0,059	C12	1,370	1,413	-0,028	0,044
C13	-0,816	-0,704	0,013	0,099	C13	-0,408	-0,289	-0,013	0,119
C14	-0,540	-0,486	0,038	0,016	C14	-0,548	-0,505	0,0287	0,0435
C15	-0,410	-0,308	0,010	0,091	C15	-0,449	-0,353	0,008	0,095
C16	-0,505	-0,488	0,002	0,015	C16	-0,439	-0,440	-0,004	-0,001
-	-	-	-	-	C17	-0,650	-0,678	-0,020	-0,029
-	-	-	-	-	N18	-0,165	-0,101	0,051	0,064
-	-	-	-	-	C19	-0,611	-0,630	-0,018	-0,019
-	-	-	-	-	C20	0,526	0,565	0,032	0,040
-	-	-	-	-	C21	-0,204	-0,169	0,014	0,035
-	-	-	-	-	C22	0,339	0,407	0,052	0,068

For MB1 inhibitor, it can be seen that the highest values of f^+ are dedicated to O1, N4, C9, O10 and C14 atoms which indicates that these atoms are more susceptible for the nucleophilic attack. However, it is apparent that the highest f^- values related to MB1 are associated with the constitutive atoms that C6, O10, C11, C12, C13 and C15, these sites are predicted to contribute in the electrophilic attack.

For MB2 inhibitor, it is evident that the highest values of f^+ are dedicated to O1, N4, C9, O10 and C14 atoms which means that these atoms are more privileged for the nucleophilic attack. However, it is apparent that the highest f^- values related to MB2 are associated with the following atoms: O1, N4, O10, C14, N18, C20 and C22, these sites are expected to participate in the electrophilic attack.

SAR results

SAR calculations have been applied and several parameters have obtained and resumed in Table 4. The polarizability (α) measures the change in the electronic distribution of the molecule with respect to the applied electric field.[23] When the polarization increases, the intrinsic molecular value increasing which makes the adsorption of the molecule into the metal surface becomes easier.[23] According to the results of Table 6, the polarizability (α) of MB2 is greater than that of MB1, which implies an excellent correlation with the inhibition potentials previously reported.

The hydrophobicity coefficient (log*P*) is an important parameter to measure the anticorrosive efficiency of a molecule. As the hydrophobicity increases, the water solubility of the molecule decreases. Therefore, the electronic transport to the metal surface becomes slower and the adsorption of the inhibitor molecule into the metallic surface will be weak.[23] As shown in Table 6, log P increased as follows: MB1 < MB2, this result doesn't correlate with the experimental results.

The hydration energy (HE) of a molecule measures the degree of dissolution. Negative values of the hydration energy (HE) indicate an exothermal dissolution.[23] The increase in the hydration energy (HE) leads to the increase in the efficiency of the molecule.[23] Regarding the (HE) data listed in Table 6, the trend in this parameter follows the order: MB1 > MB2, which doesn't validate the experimental outcomes.

The larger the surface area (SA) of the inhibitor molecules, the larger the surface adsorbed by contact and the more satisfactory the effectiveness of the inhibitor.[23] As can be seen from Table 6, the surface area (SA) of MB2 is larger that of MB1 which can result higher surface coverage and

therefore lead to higher inhibition efficiency. This result is in excellent correlation with the experimental findings.

The molecular volume (*V*) illustrates possible coverage of a metallic surface by the inhibitor. The compound having a large molecular volume value has the highest surface coverage and therefore could give high protection performance to the metal surface.[23] The inhibition efficiency shifts to higher values when the molecular volume increases due to the improvement of the contact gap between the molecule and the surface.[23] A comparison of molecular volume (*V*) values across structures revealed the order: MB2 > MB1. Therefore, the order of inhibition efficacy would preferentially be such as MB2 > MB1, which is well consistent with the experimental inhibition effectiveness data earlier reported.

Table 6
SAR parameters of MB1 and MB2 inhibitors

SAR parameter	MB1	MB2
HE	-2.616	-5.686
log*P*	1.060	2.526
V	713.314	896.574
SA	447.126	539.062
α	24.579	33.530

CONCLUSION

In the course of this rigorous investigation, a comprehensive exploration has been undertaken employing Density Functional Theory (DFT) calculations both in the gaseous and aqueous phases. Utilizing the B3LYP functional in tandem with distinct basis sets, as previously delineated, has yielded profound molecular insights that significantly enhance our comprehension of the experimental inhibition activity exhibited by the morpholinyl Mannich bases under study. Through the meticulous analysis of the results and subsequent discussions, the following salient conclusions emerge:

Global reactivity descriptors encompassing critical factors like dipole moment, energy gap, hardness, and softness demonstrate a discernible relationship with the experimental inhibition efficiency. This correlation underscores the pertinence of these descriptors in gauging the inhibitory potential of the studied compounds.

HOMO energy (E_H) and electronegativity (χ) are found to lack a direct correlation with the experimental inhibition efficiency order. This nuanced insight highlights the complexity of the interplay between molecular properties and inhibition efficacy.

The application of Fukui functions has yielded an insightful comprehensive reactive scheme, effectively delineating the active atomic sites responsible for orchestrating electronic transfers. This scheme augments our understanding of the intricate mechanistic processes underlying inhibition effectiveness.

In a notable alignment with experimental findings, SAR parameters encompassing *V*, SA, and α have substantiated the empirical sequence of inhibition efficacy. This validation reinforces the utility of these parameters as reliable indicators of inhibitory performance. In contrast, however, the hydration energy (HE) and log*P* have not demonstrated the same alignment.

REFERENCES

1. S. D. Zhu, A. Q. Fu, J. Miao, Z. F. Yin, G. S. Zhou and J. F. Wei, *Corros. Sci.*, **2011**, *53*, 3156–3165.
2. K. R. Ansari, M. A. Quraishi and A. Singh, *Measurement*, **2015**, *76*, 136–147.
3. R. Solmaz, E. A. Sahin, A. Doner and G. Kardas, *Corros. Sci*., **2011**, *53*, 3231–3240.
4. T. H. Muster, A. E. Hughes, S. A. Furman, T. Harvey, N. Sherman, S. Hardin, P. Corrigan, D. Lau, F. H. Scholes, P. A. White, M. Glenn, S. J. Garcia and J. M. C. Mol, *Electrochim. Acta*, **2009**, *54*, 3402–3411.
5. C. O. Gretir, B. Mihci and G. Bereket, *J. Mol. Struct.*, **1999**, *488*, 223–231.
6. A. Khiouani, S. E. Hachani, I. Selatnia, N. Nebbache and S. Makhloufi, *J. Indian Chem. Soc*., **2022**, *99*, 100497.
7. H. H. Rasul, D. M. Mamad, Y. H. Azeez, R. A. Omer and K. A. Omer, *Comput. Theor. Chem.*, **2023**, *1225*, 114177.
8. K. H. Rashid, K. F. AL-Azawi, A. A. Khadom, A. S. Jasim and M. M. Kadhim, *J. Mol. Struct*., **2023**, *1287*, 135661.
9. I. B. Obot and S. A. Umoren, *Int. J. Electrochem. Sci.*, **2020**, *15*, 9066–9080.
10. Y. Chen, Z. Chen and Y. Zhuo, *Materials*, **2022**, *15*, 4218.
11. A. Lesar and I. Milosev, *Chem. Phys. Lett*., **2009**, *483*, 198–203.
12. T. Koopmans, *Physica E*, **1934**, *1*, 104–113.

13. R. G. Pearson, *Inorg. Chem.*, **1988**, *27*, 734–740.
14. R. G. Pearson, *J. Chem. Edu*., **1987**, *164*, 561–567.
15. K. Ramya, R. Mohan, K. K. Anupama and A. Joseph, *Mater. Chem. Phys*., **2015**, *149-150*, 632–647.
16. K. Ramya, K. K. Anupama and K. M. Shainy, *Egypt. J. Petrol.*, **2017**, *26*, 421–437.
17. I. B. Obot and Z. M. Gasem, *Corros. Sci.*, **2014**, *83*, 359–366.
18. A. Bouoidina, F. El-Hajjaji, A. Abdellaoui, Z. Rais, M. Filali Baba, M. Chaouch, O. Karzazi, A. Lahkimi and M. Taleb, *JMES*, **2017**, *8*, 1328–1339.
19. A. Dutta, K. S. Saha, P. Banerjeeb and D. Sukul, *Corros. Sci.*, **2015**, *98*, 541–550.
20. M. Dehdab, M. Shahraki and S. M. Habibi-Khorassani, *Amino Acids*, **2016**, *48*, 291–306.
21. I. Lukovits, E. Kalman and F. Zucchi, *Corrosion*, **2001**, *57*, 3–8.
22. T. Lu and F. Chen, *J. Comput. Chem.*, **2012**, *33*, 580–592.
23. A. M. Al Sabagh, N. M. Nasser, A. A. Farag, M. A. Migahed, A. M. F. Eissa and T. Mahmoud, *Egypt. J. Petrol*., **2013**, *22*, 101–116.